Exciton self-trapping at an isoelectronic center in silicon

Gordon Davies, M. Zafar Iqbal,* and E. C. Lightowlers
Physics Department, King's College London, Strand, London WC2R 2LS, United Kingdom
(Received 11 April 1994)

We show that an exciton is self-trapped at the well-known ABC optical center in silicon by a lattice relaxation of 35±3 meV. The self-trapping arises from the electron component of the exciton, which is highly localized within about one atomic spacing of the core of the optical center. The effects of compressive stresses on the photon energy and polarization of the ABC luminescence band are reported for temperatures of 4.2 and 20 K. They can be fitted accurately by expressing the bound exciton states as perturbed band states of the silicon. The deformation potentials required for the hole component of the exciton are very close to those of the perfect lattice, consistent with the hole being only weakly localized on the center, while the deformation potential of the electron is modified by its strong localization. The center is thus a particularly clear case of a "pseudoacceptor" isoelectronic center, with properties that appear to be highly localized or weakly localized depending on the particular measurement. The importance of the lattice relaxation in binding the exciton implies that symmetry determinations by optical measurements may not measure the symmetry of the unrelaxed core of the defect.

I. INTRODUCTION

Isoelectronic centers in semiconductors have no long-range Coulomb attraction which can bind electrons or holes. However, it has long been recognized that carriers may be weakly bound by the difference between the electronegativity of the impurity atom(s) and the host atoms,[1] decreased through screening by the dielectric response of the lattice.[2] If one carrier can be trapped, then a carrier of the opposite sign may be trapped in the Coulomb field of the first, and in favorable cases the excited states of the second particle form an effective-mass-like "Rydberg" series. One example is the Be-related center in silicon, which can bind a hole in pseudoacceptor states when an electron has been trapped in the short-range potential.[3] As a result of the weak binding, the luminescence from isoelectronic centers usually occurs close to the energy of the electronic gap, and the excited states are described as a bound exciton. For a weakly bound exciton in an indirect-gap semiconductor, the luminescence spectrum is expected to show coupling to wave-vector-conserving phonons of the perfect lattice, but otherwise little interaction is expected between the diffuse exciton and the lattice. This is usually the case, although the photoluminescence spectra of some centers (e.g., GaP:Bi) show strong phonon sidebands.[4] Recently the role of lattice relaxation has been raised again in two different contexts. In one, Ham and Leung[5] have shown that the hole-lattice coupling can invert the order of the energy levels for excitons bound to neutral acceptors, as long as the hole orbitals are sufficiently small. For excitons bound to Si:Ga, the hole Bohr radius would be required to be only 1 nm (four atomic spacings). In the second case, Bouma *et al.*[6] have shown that there is an appreciably vibronic interaction between two electronic states of an exciton bound to GaP:N, and have deduced a value of 1.9 nm for the effective Bohr radius of the exciton.

The purpose of this paper is to show that for at least one isoelectronic center in silicon, lattice relaxations play a dominant role in *binding* the exciton. We will show that, when an exciton is trapped on the center, it initiates a lattice relaxation which reduces the energy of the center by an amount closely equal to the binding energy of the exciton—the exciton can be regarded as self-trapped. The self-trapping mechanism is familiar in other contexts (e.g., the self-trapped hole in an alkali halide), but to our knowledge has not been applied to isoelectronic centers in silicon. The self-trapping occurs specifically from the electron component of the exciton, which will be shown to be located within about one atomic spacing of the core of the optical center. The hole is then weakly localized, and has characteristics derived from the valence-band maxima. As a result the optical center may appear to be a "deep" center or a "shallow" center, depending on which particle is involved in the measurement. The isoelectronic center discussed here is known as the ABC center, characterized by two zero-phonon lines, A at 1122.3 meV at low temperature and C lying 3.0 meV higher (Fig. 1).[7] The chemical origin of the center is uncertain. Alt and Tapfer[8] have shown that the A line is shifted by 0.22 meV to higher energy in ^{15}N-implanted silicon compared to ^{14}N, implying the presence of at least one nitrogen atom in the center. Tajima[9] has shown that in a series of epitaxial silicon layers there was a linear relationship between the concentration of nitrogen and the intensity of luminescence in the A line (normalized with respect to the free-exciton emission). Sauer, Weber, and Zulehner[10] have established a similar dependence of the luminescence intensity in crucible and zone-refined silicon crystals which have been deliberately doped with nitrogen. The identity of any group-III element involved in an isoelectronic pairing is not clear—the ABC lines are readily observed in Al-doped silicon but there are no unambiguous data linking Al to the center.

The luminescence transitions from the levels A and C have relative intensities I given by the Boltzmann expression $I_C/I_A = P_C/P_A \exp(E/kT)$, with an activation energy $E = 3.2 \pm 0.1$ meV and relative transition probabilities

$P_C/P_A \sim 1$.[7] In broad agreement, absorption measurements on a 3 cm length of float-zone Al-doped silicon have given a ratio of $P_C/P_A = 1.40 \pm 0.05$.[11] Another excited state B lies ~ 0.8 meV below A, but transitions from B are forbidden in the unperturbed center. B is induced by magnetic field perturbations[7] or by externally applied strains (Sec. V below). The Zeeman effect on the luminescence is consistent with the symmetry of the optical center being C_{3v}.[7] Now, in spherical symmetry an exciton formed from a spin $s = \frac{1}{2}$ electron and a $j = \frac{3}{2}$ hole would form a $J = 2$ and $J = 1$ pair of levels. In the C_{3v} symmetry of the center the $J = 2$ exciton splits, with the $J_z = \pm 1$ and ± 2 levels being observed as the excited states of the A and B lines. The $J = 1$ exciton states produce the C luminescence line.[7]

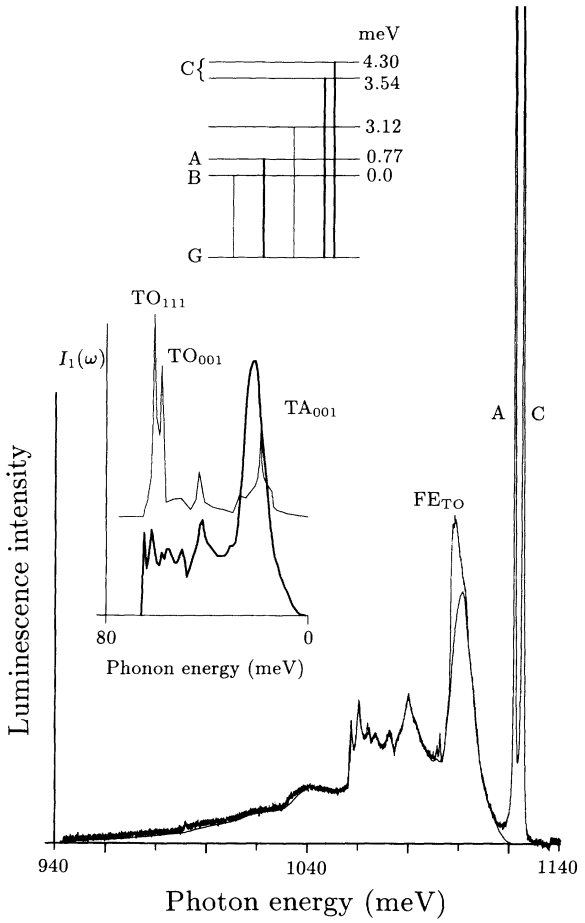

FIG. 1. The curve with noise shows the photoluminescence recorded at 20 K from the ABC center. The integrated intensity in the A line is five times larger than in the C line. Superimposed on the band is emission from free excitons with the creation of one transverse optic phonon ("FE_{TO}"). The smooth line through the data is a fit to the band shape using $S = 1.07$ and the one-phonon band shape shown on the same scale by the thicker line in the inset. The thinner line in the inset shows the density of phonon states of perfect silicon as calculated by Zdetsis (Ref. 14). Some critical points are labeled, and the spectrum is displaced vertically for clarity. The energy-level diagram at the top shows the ground state G of the center and the calculated energies of the five lowest-energy exciton states. Allowed electric-dipole transitions are indicated by the thicker vertical lines and forbidden transitions by the thinner lines. The diagram is not to scale.

No absorption lines have been detected to higher energy than the C line,[11] but photoluminescence excitation (PLE) measurements have shown that there are several excited states 22–35 meV to higher energy.[12] In the PLE work luminescence from the center was detected using the A line, precluding measurements closer than 10 meV to the A line. Consequently, the intensities of these higher-energy lines relative to the A and C lines are unknown. The higher excited states have been described in terms of a pseudoacceptor model, in which an electron is trapped first by the local field of the center, and a hole is then bound in the Coulomb field of the electron.[12] We will present independent evidence here for the pseudoacceptor model, but will also show that some electron states are predicted to lie close to the energies of the higher excited states.

Since the self-trapping deformation of the isoelectronic center can only exist as long as the exciton is bound to the center, the deformation is removed when the exciton annihilates in a luminescence transition. We can therefore determine the importance of this mechanism from the properties of the vibronic band associated with the luminescence. This procedure will be carried out in Sec. III, where we will show that symmetry-conserving deformations account for essentially all the binding energy. However, to explain the observed energy levels other exciton, a small trigonal distortion must be introduced, which results in major changes to the wave function of the exciton. In Sec. IV we will model the symmetry lowering by using a local strain field to perturb the conduction- and valence-band extrema. Since we are emphasizing the role of deformations at the center, we investigate the effects of further, controlled, deformations produced by externally applied strains. In Sec. V we show that the model accurately describes the effects of the external stresses using a small number of parameters which have values very close to those derived from the deformation potentials of the band extrema of the perfect crystal. We also show that a suitable external strain can neutralize the self-binding strain and quench the luminescence. In Sec. VI the results are shown to imply that the electron component of the exciton is tightly bound, and is responsible for the self-trapping relaxations, while the hole is only weakly bound and produces the band-edge effects. We begin by outlining the experimental details.

II. EXPERIMENTAL DETAILS

We have carried out extensive tests to maximize the luminescence intensity from the ABC system. Unfortunately, the concentration of ABC centers required for strong luminescence (estimated at less than $\sim 10^{13}$ cm^{-3} by Weber, Schmid, and Sauer[7]) is sufficiently low that it is difficult to define the optimum conditions for producing the centers. Heating float-zone Al-doped silicon at 700 °C in an Ar atmosphere always produced the luminescence in the A line, whether Fe or Cu was also introduced or no impurity was deliberately introduced. At

700 °C the duration of the heating was not critical (between 5 and 60 min), nor was the rate of cooling the samples. Heating at or above 800 °C produced lower A line luminescence, in agreement with Alt and Tapfer[8] (who annealed N-implanted samples). Heating at 1000 °C in a nitrogen atmosphere produced a very weak A line regardless of the presence of Al. For this work samples were prepared by heating float-zone crystalline silicon, with Al concentrations of 4.6×10^{15} cm^{-3}, at 700 °C for about 30 min.

Uniaxial stresses have been applied with the samples either immersed in liquid helium at 4.2 K or in an adapted Oxford Instruments helium-flow cryostat at 20 K. Luminescence was excited by an argon laser, operating typically at about 50 mW/mm^2 at the sample, and was analyzed using a Nicolet 60SX Fourier-transform spectrometer fitted with a cooled North Coast germanium detector. For accurate polarization studies the sample was excited at the back face by the above-band-gap radiation and the luminescence was detected through the front face. The edges of the sample were covered to reduce spurious refraction of luminescence into the spectrometer since these effects depolarize the spectra. The throughput of the spectrometer is about 20% smaller when the electric vector of the light is perpendicular to the stress axis than when it is parallel to the stress axis.

III. VIBRONIC PROPERTIES

The suggestion that an exciton may be self-trapped at the ABC center can be tested by applying the standard theory of vibronic band shapes to the luminescence band. The relevant vibronic theory is contained in Ref. 13 but is outlined here for convenience.

We will write the vibrational potential V_g for the ground state of the isoelectronic center as $V_g=\frac{1}{2}\sum_i m_i\omega_i^2Q_i^2$, where m_i is the effective mass of the vibration with angular frequency ω_i and coordinate Q_i, and the center is in equilibrium when all $Q_i=0$. We define the energy of one bound exciton state to be E when all $Q_i=0$. The simplest form of the adiabatic potential in this excited state is $V_e=E+\frac{1}{2}\sum_i m_i\omega_i^2Q_i^2+\sum_i a_iQ_i$, where the last term represents the interaction between the exciton and the lattice. Only the interaction linear in the Q_i is used here (since the exciton-lattice interaction will be seen to be small at the ABC center). The potential excludes both Jahn-Teller interactions and interactions between the different exciton states—neglecting them will be justified later in this section. The minimum in V_e occurs when the $Q_i=-a_i/m_i\omega_i^2$. At the minimum $V_e=E-E_r$, where the relaxation energy E_r is

$$E_r=\sum_i a_i^2/2m_i\omega_i^2 . \tag{3.1}$$

When luminescence occurs the exciton is annihilated. The change in the equilibrium configuration back to $Q_i=0$ produces a vibronic sideband as well as a zero-phonon line in the luminescence band.[13] The relaxation energy E_r is given by the difference between the zero-phonon energy E_z and the energy E_c of the centroid of the luminescence band:

$$E_r=E_z-E_c . \tag{3.2}$$

In the limit of low temperature all the bound excitons occupy the nonluminescent, lowest-energy B state. With increasing temperature the luminescence initially increases in intensity and by 20 K it is sufficiently strong to yield spectra with a good signal-to-noise ratio (Fig. 1). At this temperature ~35% of the centers are in the luminescing A state, but the C line has still only about $\frac{1}{5}$ the intensity of the A line. There is some superimposed emission, labeled FE_{TO}, from free excitons involving one transverse optic phonon. The centroid energy obtained by direct integration of the entire luminescence band (ignoring the irrelevant FE features) is $E_c=1087.8\pm3$ meV. Hence from Eq. (3.1) the relaxation energy is $E_r=35\pm3$ meV, taking $E_z=1122.8$ meV as the mean zero-phonon energy.

To investigate which vibrational modes contribute to the relaxation we define the Huang-Rhys factor S_i for the mode of quantum $\hbar\omega_i$ as the intensity (relative to the zero-phonon intensity) of the vibronic sideband involving one phonon of mode i. The relaxation energy E_r^i in that mode is then[13]

$$E_r^i=S_i\hbar\omega_i \quad \text{and} \quad E_r=\sum_i S_i\hbar\omega_i . \tag{3.3}$$

To find S_i we break the band shape into luminescence processes involving $1,2,\ldots,n$ phonons. The n-phonon process can be obtained by any combination of n phonons, so that the band shape $I_n(\omega)$ of the n-phonon sideband at a frequency ω from the zero-phonon line is[13]

$$I_n(\omega)=\int dx\, I_1(x)I_{n-1}(\omega-x) , \tag{3.4}$$

where the integral runs over all the mode frequencies. The total intensity in the n-phonon sideband is related to that in the zero-phonon line I_0 by

$$\int d\omega\, I_n(\omega)/I_0=S^n/n! \quad \text{where } S=\sum_i S_i . \tag{3.5}$$

The zero-phonon line contains a fraction $\exp(-S)$ of the total band. From our spectra we estimate $S=1.07$, similar to $S\sim1.25$ given by Weber, Schmid, and Sauer.[7] The simulated band shape of Fig. 1 has been calculated using Eqs. (3.4) and (3.5) with $S=1.07$ and with the one-phonon spectrum shown in the inset of the figure. The band shapes associated with A and C have been assumed to be identical so that the total spectrum is the weighted sum of the two, displaced in energy by the 3.2 meV separation of A and C. The assumption of identical phonon sidebands for the A and C zero-phonon lines is justified by their similarity at low and high temperature, apart from any broadening produced by the superimposition of the two bands.

From $I_1(\omega)$ and Eq. (3.3) we find $E_r=35.5$ meV, in close agreement with the determination from the centroid. The major contribution to $I_1(\omega)$ is centered on $\hbar\omega\sim21$ meV and cannot be assigned to any critical point, as shown by the comparison with the density of phonon states for perfect silicon.[14] $I_1(\omega)$ deviates considerably from the expectation for a weakly bound exciton in sil-

icon, where only transverse acoustic (18.4 meV), longitudinal optic (56.2 meV), and transverse optic (58.0 meV) wave-vector-conserving phonons are seen.

The simple theory used here assumes no Jahn-Teller interactions and no vibronic interactions between the many nearly degenerate exciton states. In practice, because the luminescence spectrum monitors the vibronic properties of the nondegenerate ("vacuum") ground state and because the Huang-Rhys factor S is only of the order of unity, the band-shape calculation would fit the experimental spectrum even if these interactions did occur in the excited states.[15] However, under high uniaxial stresses, as reported in Sec. V, the vibronic band retains the same shape as at zero stress, and its polarization follows that of the zero-phonon structure. These are the characteristics of a vibronic band produced by vibrations which are totally symmetric in the point group of the center (cf. Ref. 16), and so the simple theory used here is probably the most suitable one. In any case, very similar estimates would be made for the relaxation energy for any type of interaction.

In this section we have found that the lattice relaxation in the excited states involves phonons from all parts of $\mathbf{k}$ space, and not simply the wave-vector-conserving phonons, and has a magnitude $E_r = 35 \pm 3$ meV. This self-trapping energy forms part of the binding energy of the exciton to the center. The total binding energy for the exciton in the A excited state is the difference between the energy of a static free exciton (1155.2 meV) and of the A state (1122.3 meV as $T \to 0$), or 32.9 meV. Clearly, the experimentally observed self-trapping energy is at least a major contributor to the binding energy of the exciton to the ABC center.

IV. MODELING THE EXCITED STATES

In optical measurements the symmetry of the ABC center is observed to be trigonal (Sec. I). In this section we will derive the effective size of the trigonal distortion from the measured energy separations and relative luminescence intensities of the ABC zero-phonon lines. We will represent the hole and electron by the valence- and conduction-band extrema, which will be perturbed by the local trigonal field. The general method has been used by many workers.[17,18]

The electron states are constructed from the six conduction-band minima located along the $\langle 001 \rangle$ axes in wave-vector space. In T_d symmetry these six states transform as the A_1, E, and T_2 irreducible representations, and have different energies as a result of their different interactions with the central cell. Anticipating the uniaxial stress results of Sec. V, for the ABC center we require the A_1 state to be the lowest in energy.

The hole states used for the bound exciton are the $\mathbf{k}=0$ valence-band states for the heavy- and light-mass states, and for the spin-orbit split-off state with $E_{SO} = 44$ meV higher hole energy. This state must be included since appreciable interactions between spin-orbit-split states are produced by the applied stresses of Sec. V.

If the exciton is bound on a T_d center the hydrostatic component of the lattice relaxation perturbs the energy of the electron and hole states, but produces no mixing of states. The states are mixed by the symmetry-lowering axial perturbation. We represent the axial perturbation of the center by a uniform strain field (which is some mean value averaged over the electron and hole spatial extents), so that the responses of the electron and hole are given by the deformation potentials of the valence-band and conduction-band extrema. For simplicity in comparing with the experimental data of Sec. V, the trigonal strain field will be described by an equivalent uniaxial stress of magnitude s_i.

The orbital parts of the valence band are represented by three states, p_x, p_y, p_z, which are degenerate when the spin-orbit interaction is ignored. These states are perturbed by stresses according to the standard matrix[19] for functions transforming as the T_2 irreducible representation in T_d symmetry:

$$\begin{bmatrix} a_h(s_{xx}+s_{yy}+s_{zz}) & Cs_{xy} & Cs_{zx} \\ +B(2s_{xx}-s_{yy}-s_{zz}) & a_h(s_{xx}+s_{yy}+s_{zz}) & Cs_{yz} \\ Cs_{xy} & +B(2s_{yy}-s_{zz}-s_{xx}) & a_h(s_{xx}+s_{yy}+s_{zz}) \\ Cs_{zx} & Cs_{yz} & +B(2s_{zz}-s_{xx}-s_{yy}) \end{bmatrix} . \tag{4.1}$$

The effect of spin-orbit interaction is to split the six hole states (formed from the three p states each with two spin states) into the $j=\frac{3}{2}$ and $j=\frac{1}{2}$ states with the linear combinations given in the Appendix. To fit the measured effects of stress on the indirect energy gap requires[20]

$$\begin{aligned} &a_e - a_h = 7.8 \text{ meV/GPa}, \\ &B = 22.6 \text{ meV/GPa}, \quad C = 52.5 \text{ meV/GPa}, \end{aligned} \tag{4.2}$$

where a_e is the change in the energy per unit hydrostatic stress of the electron state of A_1 representation in the T_d point group.

The electron and hole states localized in the bound exciton can couple through an exchange energy Δ. We only consider an exchange interaction between the lowest (A_1) electron valley orbit level and the hole states, on the grounds that the E and T_2 levels are not directly observed in our measurements (and the interaction probably diminishes for increasingly excited states, as would be expected for increasingly delocalized states).[12] The quantitative effects of Δ on the electron and hole states are tabulated in the Appendix.

This formalism allows us to calculate the response of the exciton states to any stress. The eigenvalues of the matrices in the Appendix give the changes in energy of the states, and the eigenvectors give the appropriate

linear combinations of the basis states. From the eigenstates we can calculate the optical spectra. The relevant electron orbital state transforms in T_d as A_1 and so transitions to the p_x valence-band states are allowed only with x polarization, and with equal intensity under y and z polarizations to the p_y and p_z states, respectively.

The trigonal distortion of the ABC center is introduced by a $\langle 111 \rangle$ stress of magnitude s_i. To calculate the effect of s_i on mixing the band edges, only the symmetry-reducing components of s_i are required (equivalent to setting $a_e - a_h = 0$). The two parameters Δ and s_i are then adjusted to give the best fit to the observed energy splittings of the ABC center. Qualitatively, a small stress s_i splits the $J=2$ and $J=1$ states into $J_Z = 0, \pm 1, \pm 2$ states, where the quantization axis Z is the trigonal axis. The $J_Z = \pm 2$ states are the lowest for the ABC center, producing a lowest-energy doublet from which electric-dipole transitions are forbidden. In the experiments (Secs. I and V) this state is 0.8 ± 0.05 meV below the $J_Z = \pm 1$ A level. Optical transitions are allowed (with, from the model, about equal intensity) from the two higher $J_Z = 0, \pm 1$ levels. Only one transition is seen (line C) but with the relatively large full width at half height of 0.5 meV and centered on 3.2 meV above line A. We assume that the $J_Z = 0, \pm 1$ levels lie about 2.9 and 3.4 meV above the A state, so that their centroid is at the position of line C.

The values of Δ and s_i which give the best fit to the three energy separations are

$$\Delta = 1.145 \text{ meV} \quad \text{and} \quad s_i = 94 \text{ MPa} , \tag{4.3}$$

where we emphasize that the deformation potentials of the perfect lattice have been used, and s_i corresponds to a tensile stress along the $\langle 111 \rangle$ axis. These parameters can be verified from the results of applying external stresses, as shown in Secs. V A and V B. The parameters predict that the B line is 0.77 meV below the A line (cf. 0.8 ± 0.05 meV from experiment), and that the C line is made up of two almost equal-intensity lines centered 3.15 meV above A (cf. 3.2 meV from experiment). The transition probabilities for the C and A lines are calculated to be $P_C/P_A = 1.63$, compared with experimental values derived from luminescence data of ~ 1 (Ref. 7) and 1.58 ± 0.05 (Ref. 11) and from absorption data of 1.40 ± 0.05.[11] The model also predicts a state to lie 2.39 meV above A. Transitions from this state are predicted to be forbidden, but can be induced by magnetic fields, and a magnetically induced transition has been observed 2.6 meV above A.[11]

The energy separations of the lowest excited states of the ABC center and the relative strengths of transitions from them are thus very well described using this model. The axial deformation of the ABC center is small (equivalent to strain tensor components of only $e_{xy} = e_{yz} = e_{zx} = 10^{-4}$), and in this calculation it increases the exciton binding by only about 2 meV relative to the T_d center, a small effect compared to the total lattice relaxation which reduces the energy by $E_r = 35$ meV (Sec. III). We do not know that the equivalent strain used in the model actually corresponds to a real deformation of the center, but we will show in Sec. V B that it can be neutralized by an opposite crystal strain.

V. EFFECTS OF EXTERNAL STRESS

A powerful way to probe the properties of the bound exciton is by using externally applied uniaxial stresses. In previous work[18] the effects of uniaxial stresses on the energies (only) of the ABC lines were reported for stresses up to 150 MPa at 30 K. In the present work we have remeasured the effects of stress, but using stresses up to three times higher at both "low" (4.2 K) and "high" (20 K) temperatures, and we have measured the relative intensities and polarizations of the stress-split components.

Compressive stresses have been applied along the $\langle 001 \rangle$, $\langle 111 \rangle$, and $\langle 110 \rangle$ axes. The energies of the stress-split components are shown in Fig. 2, recorded at 20 K so that the different excited states are adequately populated. The changes in energy produced by the stresses were the same at 4.2 and 20 K for the lines common to the spectra, and agree with the earlier work[18] over the limited range of overlap. Sample stress spectra for the lowest-energy luminescence lines are shown in Figs. 3–6 for, respectively, the $\langle 001 \rangle$, $\langle 111 \rangle$, and $\langle 110 \rangle$ stress axes; these data were recorded at 4.2 K. The effect of stress on the band shape is shown in Fig. 7, recorded at 20 K for good signal-to-noise ratio.

To describe the effects of external stresses we could simply change the relevant stress tensor components in the matrices of the Appendix. However, the bound exciton may have different properties from the unlocalized crystal states. Consequently, the three stress parameters $A = a_e - a_h$, B, and C are treated as adjustable parameters. Variations in the parameters will also allow for any dependence of the binding energy on the strain,[2] and for any change in the elastic constants near the center. Thus, for the external stresses we evaluate each element in the matrices of the Appendix with the three stress parame-

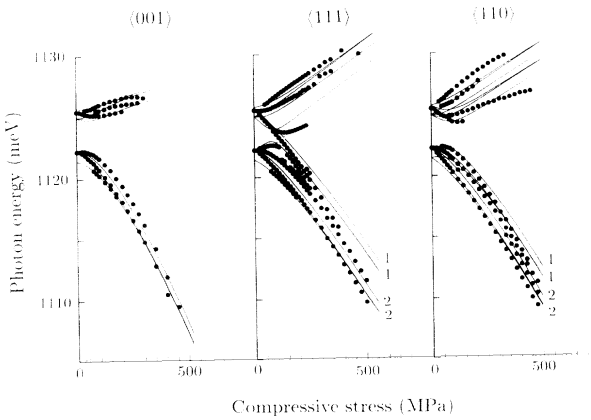

FIG. 2. Points show the energies of the optical transitions under $\langle 001 \rangle$, $\langle 111 \rangle$, and $\langle 110 \rangle$ compressions, measured at 20 K. The lines show the calculated behavior of those ABC states which are predicted to produce optically allowed transitions. The different groups of orientations producing the lowest-energy states for $\langle 111 \rangle$ and $\langle 110 \rangle$ stresses are labeled 1 and 2, as defined in Secs. V B and V C.

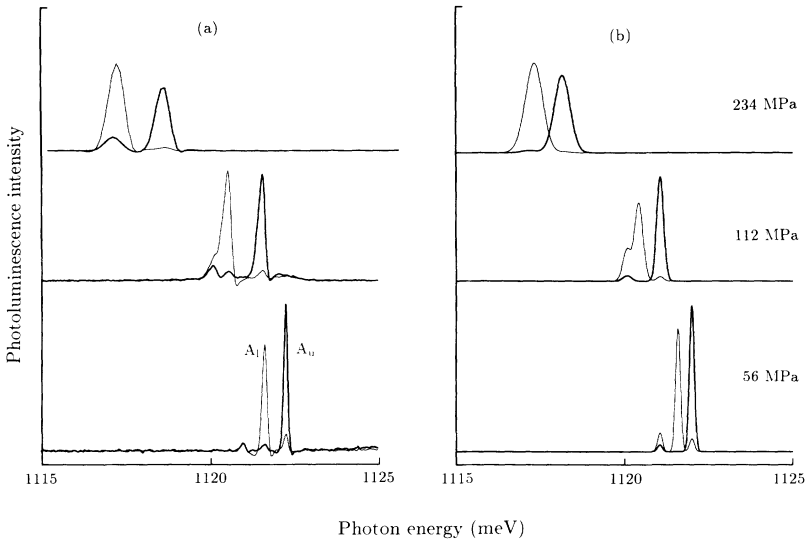

FIG. 3. (a) Spectra measured at 4.2 K under ⟨001⟩ compression of 56, 112, and 234 MPa, compared with calculated spectra (b) assuming thermal equilibrium between the exciton states and a temperature of 4.2 K. The thicker lines are for the electric vector **E** parallel to the stress **S** and the thinner lines for **E**⊥**S**. The features labeled A_l and A_u are the lower-energy and higher-energy stress-split components from the A line.

ters changed to A_e, B_e, and C_e, and add the elements for the matrices describing the internal stress s_i and the exchange interaction before diagonalizing the matrix.

This procedure leads to the calculated best fit shown by the lines in Fig. 2. The total adjustable parameters at this stage comprise Δ and s_i, derived from the zero-stress spectrum, the three main stress parameters

$$A_e = 3 \text{ meV/GPa}, \quad B_e = 17 \text{ meV/GPa}, \quad C_e = 49 \text{ meV/GPa}, \tag{5.1}$$

and the valley-orbit parameters, which only adjust the curvature of some of the energy-stress plots[21]

$$E_e = 24 \text{ meV}, \quad B_{el} = -6 \text{ meV/GPa}. \tag{5.2}$$

The three parameters A_e, B_e, C_e are accurate to about ± 2 meV/GPa, as judged by varying Δ and s_i. B_e and C_e are similar to their perfect-lattice values of Eq. (4.2), while A_e deviates more as discussed in Sec. VI. The valley-orbit parameters are inevitably less certain, perhaps to $\pm 100\%$. Nevertheless, B_{el} deviates considerably from its perfect-lattice value of -28 meV/GPa,[20] for reasons given in Sec. VI. In the remainder of this paper, no further parameters will be introduced.

Data on the intensities and polarizations of the stress-split components provide a stringent test of the modeling. The spectra have been calculated as described in Sec. IV, allowing also for the different orientations of the trigonal centers along the [111], [11$\bar{1}$], [$\bar{1}$11], and [$\bar{1}1\bar{1}$] axes, since they may become inequivalent under stress. For

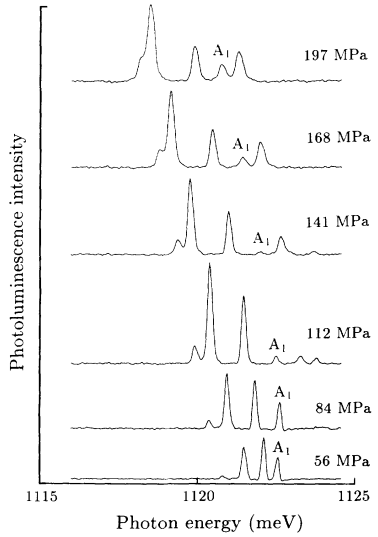

FIG. 4. Spectra measured at 4.2 K without polarization under ⟨111⟩ compression of 56–197 MPa. The spectrometer system enhances the signals with electric vector **E** parallel to the stress **S** by a factor of 1.2 relative to **E**⊥**S**. The stress-split component of the A line occurring at the centers oriented parallel to the stress is labeled A_1 and disappears near 120 MPa when the center is forced into a T_d configuration.

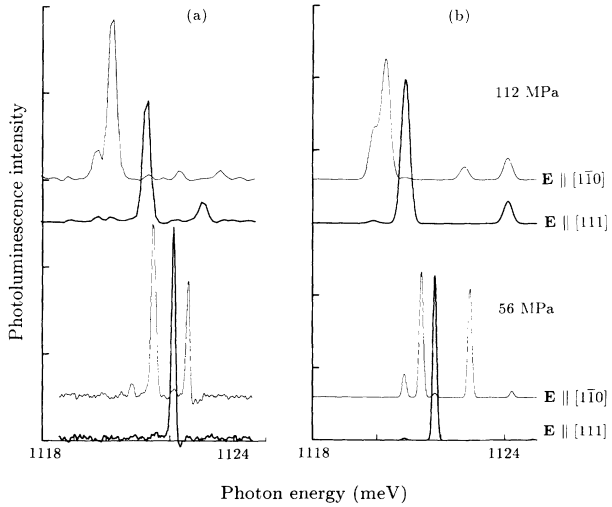

FIG. 5. (a) Spectra measured at 4.2 K under ⟨111⟩ compressions of 56 and 112 MPa, compared with calculated spectra (b) assuming thermal equilibrium between the exciton states and a temperature of 4.2 K. The thicker lines are for the electric vector **E** parallel to the stress **S** and the thinner lines for **E**⊥**S**.

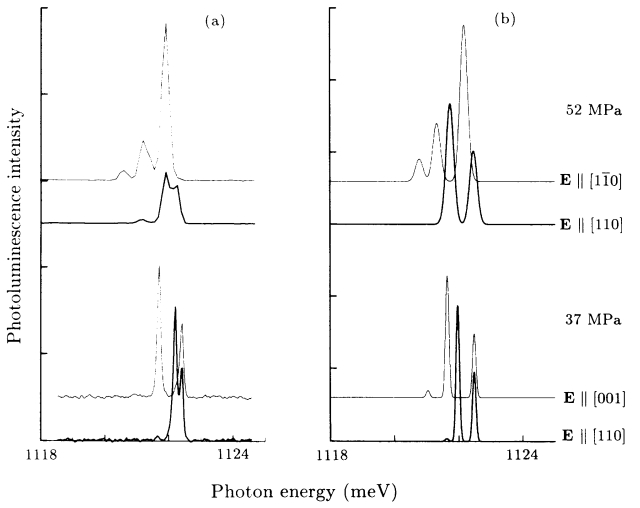

FIG. 6. (a) Spectra measured at 4.2 K under [110] compressions of 37 and 52 MPa, compared with calculated spectra (b) assuming thermal equilibrium between the exciton states and a temperature of 4.2 K. The thicker lines are for the electric vector **E** parallel to the stress **S** and the thinner lines for **E**⊥**S**. Two perpendicular polarizations are shown, **E**||[001] and **E**||[1$\bar{1}$0].

comparison with the experimental spectra shown in Figs. 3–6, which were recorded with the samples immersed in liquid helium, a temperature of 4.2 K has been assumed.

In calculating the predicted spectra, thermal equilibrium has been assumed among all the excited states for each orientation of the center, since this appears (from the measurements at 4.2 and 20 K) to be accurately obeyed in the experiments for the stresses used for Figs. 3–6. For all stress directions, transitions are forbidden

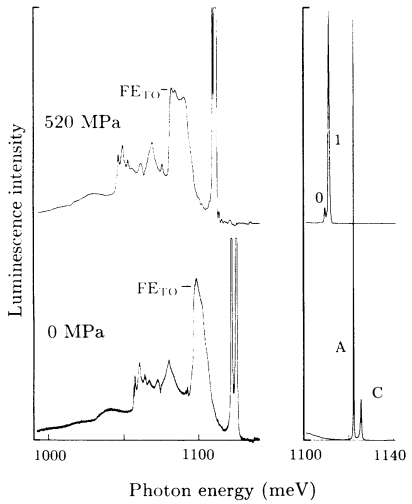

FIG. 7. Vibronic band shapes and zero-phonon regions measured without polarization at 20 K for zero stress, and for a ⟨111⟩ compression of 520 MPa. Free-exciton emission with the creation of a transverse optic phonon is labeled FE_{TO} and is superimposed on the strongest phonon sideband (see Fig. 1). The zero-phonon regions are expanded on the right to show the A and C lines at low stress and the $S=1$ and $S=0$ lines at high stress.

from the lowest-energy state (derived from one of the $J_Z=\pm 2$ states). Transitions also remain forbidden from the $J_Z=0$ state which is predicted to be 2.39 meV above the A line at zero stress (Sec. III), and whose existence is confirmed with magnetic perturbations.[10] Consequently, correct calculation of the intensities requires correct prediction of the energies as well as the admixed states for each exciton level. To aid comparison between the calculated and measured spectra, the linewidths used in calculating the spectra are as measured in the experiments. We will examine each stress direction in turn.

A. Effects of ⟨001⟩ external stress

Uniaxial stress measurements on the ABC zero-phonon lines are limited in our samples to compressions of less than about 450 MPa. With increasing stress the Al bound-exciton states decrease rapidly in energy, and as they sweep through the ABC level they quench its luminescence. This effect will be reported on elsewhere.

For external stresses along ⟨001⟩, all the ⟨111⟩-oriented centers remain equivalent. However, each orientation is subjected to symmetry-lowering stresses so that the doubly degenerate orbital excited states of the B, A, and the lower-energy part of the C doublet are all split into two components by the stress, resulting in the spectra of Fig. 3(a). To understand these spectra we focus first on the A line. The effect of a ⟨001⟩ stress on a transition between states of irreducible representations E and A_1 at a trigonal center is to split it into two components [labeled A_u and A_l for the upper and lower energy components on Fig. 3(a)].[22] One component (A_l in these measurements) should be seen only with the electric field **E** of the light perpendicular to the external stress $\mathbf{s}_e$. Our experimental spectra show a small component of A_l with $\mathbf{E}||\mathbf{s}_e$. This depolarization is an experimental artifact—it is very difficult to obtain accurately polarized luminescence spectra from silicon—and indicates the level of accuracy of our polarization data. With no stress-induced mixing of the states, component A_u would be observed four times more intensely when $\mathbf{E}||\mathbf{s}_e$ than when $\mathbf{E}\perp\mathbf{s}_e$.[22] Already by 56 MPa stress-induced mixing of the A and the C excited states has increased the intensity of A_u seen when $\mathbf{E}||\mathbf{s}_e$ and has reduced the intensity of A_u seen with $\mathbf{E}\perp\mathbf{s}_e$ [Fig. 3(a)]. By 226 MPa the luminescence with $\mathbf{E}||\mathbf{s}_e$ is predicted to have a transition probability 11 times larger than for $\mathbf{E}\perp\mathbf{s}_e$. The two signals are observed with about equal strength because at 4.2 K the population of the lower-energy states is favored. The balancing of these opposing factors is reproduced closely by the model [Figs. 3(a) and 3(b)].

The simplification of the spectra to two lines at high stress, with one polarized predominantly with $\mathbf{E}\perp\mathbf{s}_e$ and one with $\mathbf{E}||\mathbf{s}_e$, can be regarded as the effect of the large compressive stress forcing the quantization axis of the center to become closer to ⟨001⟩ as $|s_e|$ exceeds $|s_i|$. Under a sufficiently large compression the valence-band states split so that the lowest-energy hole state is orbitally nondegenerate. (It is the description of this state which requires the spin-orbit split-off valence-band state to be

included in the basis states.) The only orbital angular momentum of this state is its spin ($s=\frac{1}{2}$) which couples with the electron spin to generate a low-energy triplet ($S=1$) and a slightly higher-energy singlet ($S=0$). The transition from the higher-energy nondegenerate singlet to the ground state (both totally symmetric in the new point group of the stressed center) becomes increasingly limited to the polarization with the electric vector of the light along the new quantization axis, that is, with $\mathbf{E}\|\mathbf{s}_e$. Transitions from the lower-energy $S=1$ state become progressively forbidden. In the limit of high stress, the energy separation between the $S=1$ and $S=0$ states tends to Δ and so gives an experimental method of determining this parameter. The measurements give a high-stress splitting of ~ 1.4 meV similar to the value of 1.145 meV, Eq. (4.3), derived by modeling the energy-level structure at zero stress. (The larger observed value could be caused by a larger electron-hole overlap in the stressed case.) The same simplification to two strong components separated by 1.4 ± 0.1 meV occurs in the other stress directions at large stresses.

B. Effects of ⟨111⟩ external stress

In contrast to ⟨001⟩ compression, ⟨111⟩ stresses break the equivalence of all the orientations of the ⟨111⟩-oriented centers into two groups. Group 1 is oriented along [111]; these centers are compressed along their main axis, so that no states are split. The second group, those centers oriented with their main axis along $[11\bar{1}]$, $[\bar{1}11]$, or $[\bar{1}1\bar{1}]$, have their symmetry lowered to C_{1v}, splitting all the E states.

The internal tensile stress $\mathbf{s}_i$ of the first group is along [111]. When the external compressive stress $\mathbf{s}_e$ equals $-\mathbf{s}_i$, the bound exciton is in T_d symmetry and its five lowest-energy states become the degenerate $J=2$ set from which optical transitions are forbidden to the ground $J=0$ state. Consequently at this critical stress the A line from the [111] centers (labeled A_1 on Fig. 4) disappears; measurement gives this critical stress as $\sim 125\pm10$ MPa, compared to a predicted value from the model of 100 MPa. [The value is slightly larger than the internal stress $s_i=94$ MPa as a result of the different values of C and C_e, Eqs. (4.2) and (5.1).] Observing the critical stress gives an experimental method of determining s_i.

The response to stresses is closely reproduced by the model for stresses up to the critical stress (Fig. 5). At higher stresses the transitions from the [111]-oriented centers are considerably weaker than expected, until at the highest stresses the zero-phonon structure is almost entirely derived from the "singlet-triplet" pair associated with the Group-2 centers ($[11\bar{1}]$,$[\bar{1}11]$, or $[\bar{1}1\bar{1}]$), Fig. 2. This effect is shown further in Fig. 7, where a 20 K spectrum is shown, first so that there is enough thermal energy to populate higher levels, and second so that the vibronic sideband can be shown at good signal-to-noise ratio. It is striking that the vibronic sideband has the same shape, and the same intensity relative to the zero-phonon lines, as at zero stress. Given the considerable stress-induced mixing of the electronic states, the similarity is a strong indication that the coupling is to phonons which are totally symmetric in the point group of the optical center, since the response to totally symmetric perturbations is independent of the linear combinations of the states.

C. Effects of ⟨110⟩ external stress

Under [110] compression, two groups of centers are created. Group 1 has trigonal axes oriented along $[111]$ and $[11\bar{1}]$, while group 2 consists of the $[\bar{1}11]$ or $[\bar{1}1\bar{1}]$ centers which are perpendicular to the stress axis. For electric vector $\mathbf{E}$ perpendicular to the stress, different spectra are expected depending on the orientation of $\mathbf{E}$. Figure 6 shows the measured and calculated spectra for $\mathbf{E}\|\mathbf{s}_e$, $\mathbf{E}\|[001]$, and $\mathbf{E}\|[1\bar{1}0]$. Again the calculation is in substantial agreement with experiment except that the strongest $\mathbf{E}\|\mathbf{s}_e$ component is predicted to shift with stress faster than observed. Note that the total intensity seen with $\mathbf{E}\|[1\bar{1}0]$ is greater than with $\mathbf{E}\|\mathbf{s}_e$ as a result of the populations in thermal equilibrium of the initial states of the transitions. At high stresses the spectra simplify into a pair of lines, which are most clearly identified as occurring from the triplet and singlet states of the centers whose trigonal axes are perpendicular to the stress (Fig. 2).

VI. DISCUSSION

We have described the exciton states in terms of admixtures of basis states written in T_d symmetry. The energy-level structure at zero stress has been fitted precisely by perturbing these states, and the two parameters (Δ and $\mathbf{s}_i$) have values which are consistent with the effects of externally applied stresses (Secs. V A and V B). The effects of external stresses have been convincingly reproduced by a model in which the bound exciton is represented by the band extrema of the perfect crystal, and the two important parameters B_e and C_e which describe the response to symmetry-lowering stresses have values which are very close to the deformation potentials of the perfect-lattice states. Note that the response to axial stresses is produced by the stress-induced splitting of states *of the hole:* the A_1 electron state cannot be split by stress. The similarity of the deformation potentials of the free and bound holes implies that the bound hole retains its valence-band character and so is not strongly localized on the center.

In contrast, an examination of the vibronic sideband implies that it derives from states which are highly localized on the center. If a plane wave of the lattice modes is to interact with a particle through the deformation potentials, the vibrational wavelength must be sufficiently long that the displacements do not average out to zero over the extent of the particle. The wave function of a particle bound to a spherically symmetric potential has a zero-angular-momentum state of low energy with a wave function ψ which decreases approximately exponentially with r, as $\exp(-r/a_0)$, the precise form depending on the potential. The interaction of a plane wave (of wave vector $\mathbf{k}$) with this state relies on the interaction integral $\int \psi^* \exp(i\mathbf{k}\cdot\mathbf{r})\psi\, d\mathbf{r}$ being nonzero. For all likely forms of

ψ the interaction integral has a maximum value for waves with $k=0$ (but for which the density of states is zero), and decreases to half the maximum when $ka_0 \sim 2$. For the ABC center, the dominant mode in Fig. 1 has an energy of $\hbar\omega \sim 21$ meV which does not correspond to any critical point in the lattice. These energies are given by lattice modes with, for example, $\mathbf{k} \sim \mathbf{k}_{\max}/2$, where $\mathbf{k}_{\max}$ is the zone-boundary value in the $\langle 001 \rangle$ direction. For this value of $|k|$, $ka_0=2$ when $a_0=0.34$ nm, i.e., between one and two atomic spacings. While the details depend on the form of the binding potential, the calculation demonstrates that the particle producing the vibronic interaction must be very highly localized.

Confirmation of the high localization comes from the Huang-Rhys factor which was found in Sec. III to be $S=1.07$. The phonon coupling is totally symmetric in the point group of the center, and so we will calculate S from the measured response A_e to hydrostatic stresses. Since we have predicted a_0 to be of the order of one atomic spacing we can represent the optical center by a cluster consisting of the four Si atoms which neighbor its core; this model has the advantage that no adjustable parameters are then required. Labeling these four neighbors as a, b, c, and d, we can denote the Cartesian components of their movements from equilibrium by $x_a, y_a, \ldots, z_d$. The totally symmetric mode with coordinate

$$Q=[-x_a+x_b+x_c-x_d+y_a-y_b+y_c-y_d +z_a+z_b-z_c-z_d]/\sqrt{12}$$

then has an effective mass equal to the mass m of one Si atom. A hydrostatic stress with components s_{xx}, s_{yy}, s_{zz} produces a movement

$$Q=2l(s_{xx}+s_{yy}+s_{zz})/3(c_{11}+2c_{12}) ,$$

where the elastic constants of the perfect lattice are used. Consequently, the change in energy per unit displacement, $a=\Delta E/Q$, can be related to the measured change in energy per unit stress, A_e of Eq. (5.1). Simplifying Eqs. (3.1) and (3.3) to the case of one effective mode of quantum $\hbar\omega$ and interaction term a, the Huang-Rhys factor is

$$S=a^2/2m\hbar\omega^3=9A_e^2(c_{11}+2c_{12})^2/8ml^2\hbar\omega^3 . \quad (6.1)$$

Evaluating with the effective vibrational quantum set equal to the value at the main peak, $\hbar\omega=21$ meV (Fig. 1) and with $A_e=3$ meV/GPa [Eq. (5.1)] gives $S=2.6$. This calculation assumes that the elastic constants are the same near the center as in the perfect lattice, that all the hydrostatic response A_e is produced by the localized particle, and, to avoid any adjustable parameters, that only four neighbors in a T_d complex move. That it produces a value of S with the same order as that observed indicates that it derives from a very highly localized particle. Since the hole is weakly localized, this particle must be the electron. One consequence of the electron being highly localized is that the measured stress parameters A_e and B_{el}, which depend on the response of the electron to hydrostatic and tetragonal stresses, respectively, will differ from the deformation potentials of the perfect lattice.

VII. CONCLUSIONS

We have shown in this paper that an exciton is bound to the ABC center primarily through the lattice relaxation it initiates. The self-trapping, and hence the vibronic sideband, is produced by the highly localized electron in the exciton. In contrast, the hole is only weakly localized, producing a pseudoacceptor. This agrees with the classification as a pseudoacceptor reached by Wagner and Sauer[12] on the basis of observing higher-energy optical transitions (Sec. I), but we note that transitions in this region are predicted in the present work from the higher valley-orbit states of the electron, E_e in Eq. (5.2). The invariance of the vibronic band shape under stress (Fig. 7), when considerable mixing occurs in the electronic states, is confirmation that the vibronic coupling is to totally symmetric modes of vibration in the point group of the center.

To explain the energy levels of the bound exciton it is necessary to perturb the hole states by introducing a small trigonal deformation. Because the electron is in an A_1 state it cannot be split by a trigonal deformation, and so our data contain no unambiguous information about the symmetry seen by the highly localized electron. The trigonal distortion could be limited to a small Jahn-Teller effect in the hole states. Alternatively, the small trigonal distortion affecting the hole could be the effect of a large deformation at the core of the center simply made small by the large radial distance of the hole. Consequently, these measurements raise the crucial question of how the "true" symmetry of the optical center (in its relaxed ground state) can be determined. Perturbations by magnetic fields and by uniaxial stresses show that the symmetry of the center plus its bound exciton is undoubtedly trigonal (Sec. I), but this need not apply to the ground state.

We have presented experimental data showing that a self-trapping deformation is important in binding an exciton to a center in silicon; the origin of any initial binding lies outside the scope of this paper. However, from spectra published in the literature we can see that self-trapping is not uncommon. Examples where the vibronic relaxation energy is close to the total binding energy are GaP:Bi (Ref. 4) and the four-Li-atom complex in Si.[23] Any bound exciton is unstable to a deformation of the lattice since the exciton's energy is lowered by the deformation, but to provide a total reduction in energy the diameter of at least one particle in the exciton must be sufficiently small that the elastic energy of the deformed region of the crystal does not become prohibitively large. We have shown that for the ABC center it is the electron which is highly localized. The concept of one tightly bound and one weakly bound particle is fundamental to the Hopfield-Thomas-Lynch model of bound excitons.[24] The data presented here provide a particularly clean example of this concept.

ACKNOWLEDGMENTS

M.Z.I. would like to thank the Commission of Europeak Communities for financial support. We also thank the Science and Research Council of the UK for supporting this work. M.Z.I. would also like to thank the group at King's College London for the hospitality extended to him during his sabbatical visit.

APPENDIX

Electron states

The six conduction-band minima transform in the T_d point group as A_1, E, and T_2. The uniaxial stress data of Sec. V are fitted with the A_1 state lowest. With $\langle 001 \rangle$ compression, a downward curvature is seen in Fig. 2 at higher stresses, as the A_1 state is repelled from a higher-lying E state which is not observed directly in these luminescence measurements. The A_1 state cannot interact under stress with the T_2 state.[21] The relevant matrix for the A_1 and E states is thus simply

	A_1	E_θ	E_ϵ
A_1	0	$-\sqrt{2}B_{\rm el}s_\theta$	$-\sqrt{2}B_{\rm el}s_\epsilon$
E_θ	$-\sqrt{2}B_{\rm el}s_\theta$	$E_e-B_{\rm el}s_\theta$	$B_{\rm el}s_\epsilon$
E_ϵ	$-\sqrt{2}B_{\rm el}s_\epsilon$	$B_{\rm el}s_\epsilon$	$E_e+B_{\rm el}s_\theta$

Here the origin of the energy is the A_1 state and the E state lies E_e above it at zero stress. In terms of the stress tensors s_{ij} defined with respect to the crystal's cube axes,

$$s_\theta=2s_{zz}-s_{xx}-s_{yy}\ ,\quad s_\epsilon=\sqrt{3}(s_{xx}-s_{yy})\ .$$

Hole states

The valence-band maxima can be written in terms of the three orbital states p_x,p_y,p_z of Sec. IV. Expressed in terms of angular momentum quantum numbers j and m_j they are

$\lvert jm_j\rangle$	function
$\lvert\frac{3}{2}+\frac{3}{2}\rangle$	$\sqrt{\frac{1}{2}}(p_x+ip_y)\uparrow$
$\lvert\frac{3}{2}+\frac{1}{2}\rangle$	$\sqrt{\frac{1}{6}}(p_x+ip_y)\downarrow-\sqrt{\frac{2}{3}}p_z\uparrow$
$\lvert\frac{3}{2}-\frac{1}{2}\rangle$	$-\sqrt{\frac{1}{6}}(p_x-ip_y)\uparrow-\sqrt{\frac{2}{3}}p_z\downarrow$
$\lvert\frac{3}{2}-\frac{3}{2}\rangle$	$-\sqrt{\frac{1}{2}}(p_x-ip_y)\downarrow$
$\lvert\frac{1}{2}+\frac{1}{2}\rangle$	$\sqrt{\frac{1}{3}}(p_x+ip_y)\downarrow+\sqrt{\frac{1}{3}}p_z\uparrow$
$\lvert\frac{1}{2}-\frac{1}{2}\rangle$	$\sqrt{\frac{1}{3}}(p_x-ip_y)\uparrow-\sqrt{\frac{1}{3}}p_z\downarrow$

Here $\uparrow$ and $\downarrow$ refer to the spin of the hole.

The electron and hole couple through the exchange interaction Δ. The electron is in an A_1 orbital state and has two spin states denoted $\uparrow$ and $\downarrow$. The following symmetric matrix describes the interaction of the 12 combined electron and hole states. The valence-band spin-orbit coupling has a magnitude 3ξ. For the internal stress at the center

$$p_\theta=(2s^i_{zz}-s^i_{xx}-s^i_{yy})B/2,$$

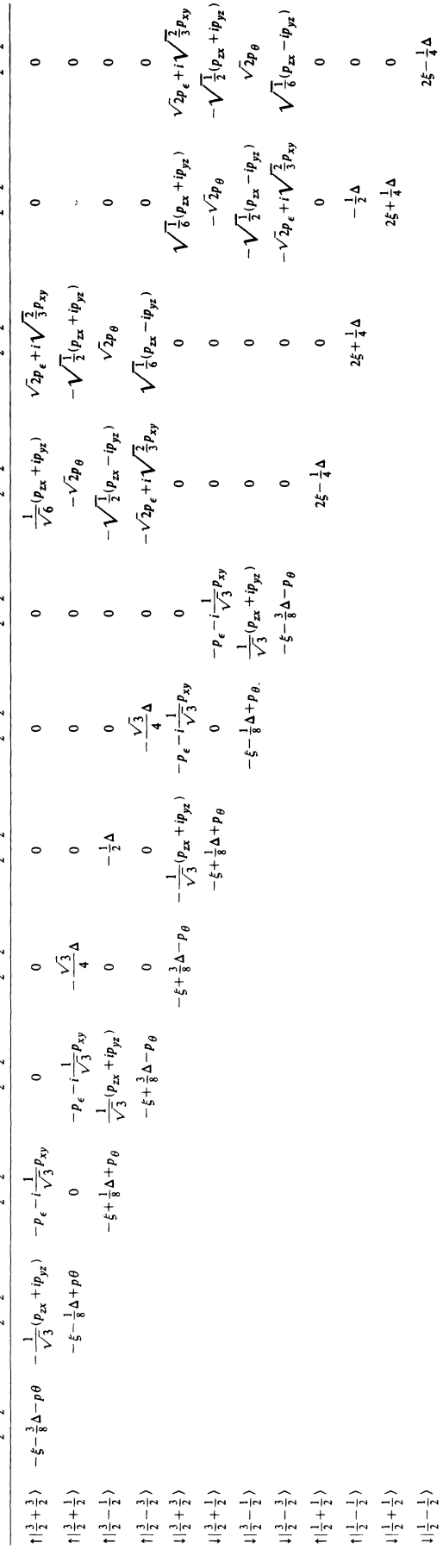

$$p_\epsilon=\sqrt{3}(s^i_{xx}-s^i_{yy})B/2, \quad p_{ij}=Cs^i_{ij} .$$

For the external stress

$$p_\theta=(2s^e_{zz}-s^e_{xx}-s^e_{yy})B_e/2,$$

$$p_\epsilon=\sqrt{3}(s^e_{xx}-s^e_{yy})B_e/2, \quad p_{ij}=C_e s^e_{ij} ,$$

and A_e $(s^e_{xx}+s^e_{yy}+s^e_{zz})$ must be added to each diagonal term.

---

*Permanent address: Semiconductor Physics Laboratory, Department of Physics, Quaid-i-Azam University, Islamabad 45320, Pakistan.

[1]Discussions of the binding mechanisms are given by, e.g., R. A. Faulkner, Phys. Rev. **175**, 991 (1968) and are reviewed extensively by P. J. Dean and D. C. Herbert in *Bound Excitons in Semiconductors,* edited by K. Cho, Topics in Current Physics Vol. 14 (Springer-Verlag, Berlin, 1979), p. 55.

[2]A. Baldereschi and J. J. Hopfield, Phys. Rev. Lett. **28**, 171 (1972).

[3]M. W. L. Thewalt, S. P. Watkins, U. O. Ziemelis, E. C. Lightowlers, and M. O. Henry, Solid State Commun. **44**, 573 (1982); D. Labrie, T. Timusk, and M. L. W. Thewalt, Phys. Rev. Lett. **52**, 81 (1984).

[4]F. A. Trumbore, M. Gershenzon, and D. G. Thomas, Appl. Phys. Lett. **9**, 4 (1986).

[5]F. S. Ham and C.-H. Leung, Phys. Rev. Lett. **71**, 3186 (1993).

[6]T. Bouma, A. J. Scholten, H. A. Zondag, Tj. Luijendijk, and J. I. Dijkhuis, Phys. Rev. B **49**, 1720 (1994).

[7]J. Weber, W. Schmid, and R. Sauer, Phys. Rev. B **21**, 2401 (1980).

[8]H. Ch. Alt and L. Tapfer, *Proceedings of the 13th International Conference on Defects in Semiconductors, Coronado, CA, 1984,* edited by L. C. Kimerling and J. M. Parsey, Jr. (Metallurgical Society of AIME, Philadelphia, 1985), p. 833.

[9]M. Tajima, Jpn. J. Appl. Phys. **21**, Suppl. 21-1, 113 (1981).

[10]R. Sauer, J. Weber, and W. Zulehner, Appl. Phys. Lett. **44**, 440 (1984).

[11]P. Mc. Colley, Ph.D. thesis, University of London, 1984.

[12]J. Wagner and R. Sauer, Phys. Rev. B **26**, 3502 (1982).

[13]M. H. L. Pryce, in *Phonons in Perfect Lattices and in Lattices with Point Imperfections,* edited by R. W. H. Stephenson (Oliver and Boyd, Edinburgh, 1966), pp. 414–425.

[14]A. D. Zdetsis, Chem. Phys. **40**, 345 (1979).

[15]For $T\times t$ coupling see N. Sakamoto and S. Muramatsu, Phys. Rev. B **17**, 868 (1978); for $T\times e$ coupling the spectra are indistinguishable from the case discussed in Sec. III of F. S. Ham, Phys. Rev. **138**, A1727 (1965); for $E\times e$ coupling see H. C. Longuet-Higgins, U. Opik, M. H. L. Pryce, and R. A. Sack, Proc. R. Soc. London Ser. A **244**, 1 (1958).

[16]Dichroism effects are described for $E\times e$ coupling by H. R. Fetterman and D. B. Fitchen, Solid State Commun. **6**, 501 (1968); for T states coupled to e and t modes by C. Escribe and A. E. Hughes, J. Phys. C **4**, L108 (1971).

[17]The generic approach was described by J. van W. Morgan and T. N. Morgan, Phys. Rev. B **1**, 739 (1970), and has been applied both to crystals, e.g., this reference, and to quantum wells, e.g., Q. X. Zhao and T. Westgaard, Phys. Rev. B **44**, 3726 (1991).

[18]G. Davies, J. Phys. C **17**, 6331 (1984).

[19]A. A. Kaplyanskii, Opt. Spectrosc. **16**, 329 (1964).

[20]L. D. Laude, F. H. Pollack, and M. Cardona, Phys. Rev. B **3**, 2623 (1971).

[21]D. K. Wilson and F. Feher, Phys. Rev. **124**, 1068 (1961).

[22]A. E. Hughes and W. A. Runciman, Proc. Phys. Soc. London **90**, 827 (1967).

[23]G. Davies, L. T. Canham, and E. C. Lightowlers, J. Phys. C **17**, L173 (1984).

[24]J. J. Hopfield, D. G. Thomas, and R. T. Lynch, Phys. Rev. Lett. **17**, 312 (1964).